Local microstructure and flow stress in deformed metals

Zhang, Xiaodan; Hansen, Niels; Nielsen, Chris Valentin

Published in:
I O P Conference Series: Materials Science and Engineering

Link to article, DOI:
10.1088/1757-899X/219/1/012053

Publication date:
2017

Document Version
Publisher's PDF, also known as Version of record

Local microstructure and flow stress in deformed metals

X Zhang[1], N Hansen[1], C V Nielsen[2]

[1]Section for Materials Science and Characterization, Department of Wind Energy, Technical University of Denmark, DK-4000 Roskilde, Denmark
[2]Department of Mechanical Engineering, Technical University of Denmark, Produktionstorvet 425, 2800 Kgs. Lyngby, Denmark

Email: xzha@dtu.dk

Abstract. The microstructure and flow stress of metals are related through many well-known strength-structure relationships based on structural parameters, where grain size and dislocation density are examples. In heterogeneous structures, the local stress and strain are important as they will affect the bulk properties. A microstructural method is presented which allows the local stress in a deformed metal to be estimated based on microstructural parameters determined by an EBSD analysis. These parameters are the average spacing of deformation introduced boundaries and the fraction of high angle boundaries. The method is demonstrated for two heterogeneous structures: (i) a gradient (sub)surface structure in steel deformed by shot peening; (ii) a heterogeneous structure introduced by friction between a tool and a workpiece of aluminum. Flow stress data are calculated based on the microstructural analysis, and validated by hardness measurement and 2D numerical simulations. A good agreement is found over a plastic strain range from ~1 to 5.

1. Introduction

Structure-strength relationships for metallic materials provide guidelines for the design and processing of engineering materials and components. An example of such relationships is the Hall-Petch equation [1,2], which relates the yield (or flow) stress to the inverse square root of the grain size, or to the spacing between boundaries in the structure that act as barriers to dislocation glide [1-3]. Specimens where such a relationship is tested are typically thermo-mechanically processed, for example, by rolling, drawing and torsion, and they are characterized as bulk materials on the assumption that the structure is homogeneous. However, during plastic deformation the stress and strain distribution in the metal may not be homogeneous, for example, where friction and wear are an inherent part of the process. Heterogeneities may also be introduced deliberately, for example by plastic deformation of a surface to increase wear and fatigue resistance of rolling components.

Characteristic heterogeneous structures can be graded or multilayer structures, and the local stress and strain distribution can be characterized by many mechanical and physical methods, such as hardness testing and methods using X-ray diffraction [4,5]. However, as the structural scale may range from the micrometer scale to the nanometer dimension, it has been suggested [4,6] to apply electron microscopy techniques, such as electron backscatter diffraction (EBSD) and transmission electron microscopy (TEM). By using such techniques it is possible to characterize microstructural parameters that can be the basis for calculation of the strength, for example, by applying the Hall-Petch

relationship. This means that it is possible to estimate the local stress distribution over multiple length scales in a heterogeneous deformation microstructure.

In the present paper we shall demonstrate the application of the microstructural techniques for two heterogeneous microstructures: (i) a gradient lamellar (sub)surface structure in steel deformed by shot peening, and (ii) a heterogeneous structure formed during a metal forming operation due to friction between the tool and a workpiece in aluminum. Calculated stress gradients are validated by microhardness measurements for the fomer case and by 2D numerical simulation for the latter case.

2. Strength-structure relationship

A number of structural parameters from microstructural analysis can be identified as strengthening parameters. These are the spacing (D) between, and the misorientation angle (θ) across, the deformation induced boundaries, where the misorientation angles are separated into low angles ($\theta < 15^o$) and high angles ($\theta \geq 15^o$), thereby defining the two main strengthening mechanisms, corresponding to dislocation strengthening and boundary strengthening, respectively.

Dislocation strengthening is typically accounted for by a Taylor strengthening [7] where, for example, the yield stress is taken to be proportional to the square root of the dislocation density stored both in dislocation boundaries and as a small fraction in the volume between boundaries. Boundary strengthening can be accounted for by a Hall-Petch relationship. The flow stress can then be estimated as the sum of these two contributions with the addition of the friction stress and a contribution from dispersed particles (in the case of Al).

However, a modification has been introduced [4] as there appears to exist an angle (β) above which the boundaries change from being penetrable to be impenetrable. This critical angle is estimated to be ~ 6° for Fe [6] and ~ 2° for pure Al [8]. It follows that the structure-strength relationship can be written:

$$\sigma - \sigma_0 - \sigma_{particle} = \left[k_{HP}^{*} \sqrt{f^{\theta>\beta}} + M\alpha G \sqrt{3b\theta^{\theta\leq\beta}(1-f^{\theta>\beta})} \right] D_{av}^{-0.5} \quad (1)$$

$$\sigma - \sigma_0 - \sigma_{particle} = k_2 D_{av}^{-0.5} \quad (2)$$

where $f^{\theta>\beta}$ is the fraction of boundaries with a misorientation angle higher than the critical value, σ_0 is the friction stress, $\theta^{\theta\leq\beta}$ is the average value of misorientation angles lower than the critical angle, β, and D_{av} is the average spacing between all boundaries measured along random intersection lines.

k_{HP} is typically determined for a polycrystalline structure subdivided by high angle boundaries ($\geq 15^o$). In the present case, boundary strengthening includes contributions from both high angle boundaries ($\geq 15^o$) and low angle boundaries ($\geq \beta$). The value of k_{HP}^{*} is larger than k_{HP} and has to be derived experimentally. This is done based on analysis of structures which have been homogeneously deformed in rolling for Fe [4] and in compression for Al. Based on these data and combined with equation (2) the following average values have been obtained: for cold-rolled Fe, $k_2 = 310 \pm 11$ MPa $\mu m^{0.5}$; for cold compressed Al, $k_2 = 112 \pm 10.5$ MPa $\mu m^{0.5}$.

3. Experimental results and validation

3.1 Shot peened low carbon steel

A low carbon steel (Fe-0.004 wt. % C) bar of diameter Ø = 12 mm, with a grain size of 40 μm has been shot peened using 0.8 mm high-carbon steel balls (0.91 wt. % C, HRC 62) for 5 min. The shot velocity was ~260 m/s and the coverage was 200 %.

Backscatter imaging and electron backscatter diffraction (EBSD) have been applied to quantify the microstructure [9-12]. The step sizes for EBSD scanning are 1000 nm, 200 nm, 120 nm, 50 nm and 20 nm, chosen according to the fineness of the deformation structure with finer map step sizes used for finer deformation structures.

Figure 1 shows the microstructure from the top surface to a position ~ 460 μm from the surface in the shot peened low carbon steel. The EBSD microstructure is consistent with the microhardness profile as shown in figure 1e, with the structure divided into three zones: Zone A (0-110 μm) has a lamellar structure parallel to the surface, with a sharp hardness increase as the surface is approached; Zone B (110-600 μm) has deformed coarse grains with dislocation boundaries and tangles with a slow hardness increase as the surface is approached; and Zone C (600 μm-) is the undeformed matrix with an almost constant hardness.

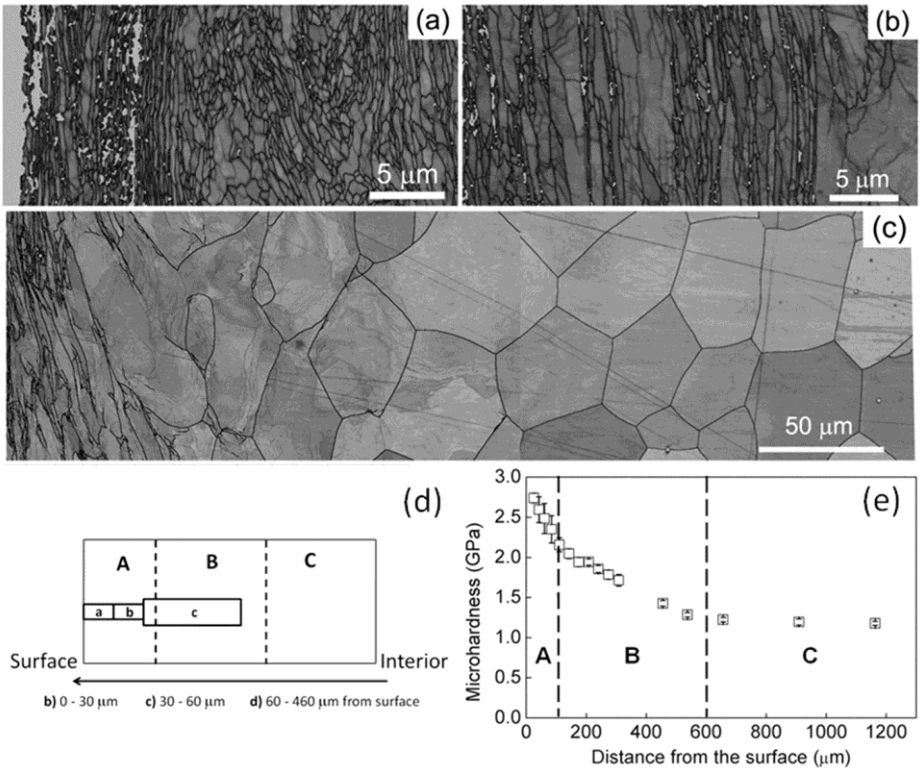

Figure 1. (a-c) EBSD microstructure (greyscale corresponding to band contrast) at the locations shown in the schematic illustration (d). Capital letters A, B and C correspond to areas marked in the microhardness distribution (e) as a function of distance from the surface in a shot-peened low carbon steel [4].

The key structural parameter, D_{av}, (see equation (2)) is given in table 1 at different distances from the surface. The calculated flow stress is shown in figure 2 as a function of the distance from the surface. Note that the maximum stress is ~ 1400 MPa at the surface, which is 6-7 times the flow stress of the undeformed steel in the interior volume. The calculated flow stress is validated by microhardness data included in figure 2, where the flow stress is converted via the relationship $HV/3.5 = \sigma_{(0.2\%)}$, and where good agreement is found. However, the microstructural parameters can be quantified up to the surface, whereas the microhardness data are limited to depths of below 25 μm from the surface. For this region we extrapolate the hardness curve of the top 300 μm area to the surface by $HV = 4830 \times d^{-0.17}$, where d is the distance to the surface and HV is the Vickers hardness determined with a load of 50g with the holding time of 20 s. Based on equation (1), D_{av} at the surface can be estimated to be ~ 70 nm.

Table 1. Average boundary spacing for shot-peened samples (SP) at different distances from the surface (data based on EBSD analysis) [4].

Location	D_{av} (nm)
10-0μm_SP	115
20-10μm_SP	181
40-20μm_SP	260
60-40μm_SP	360

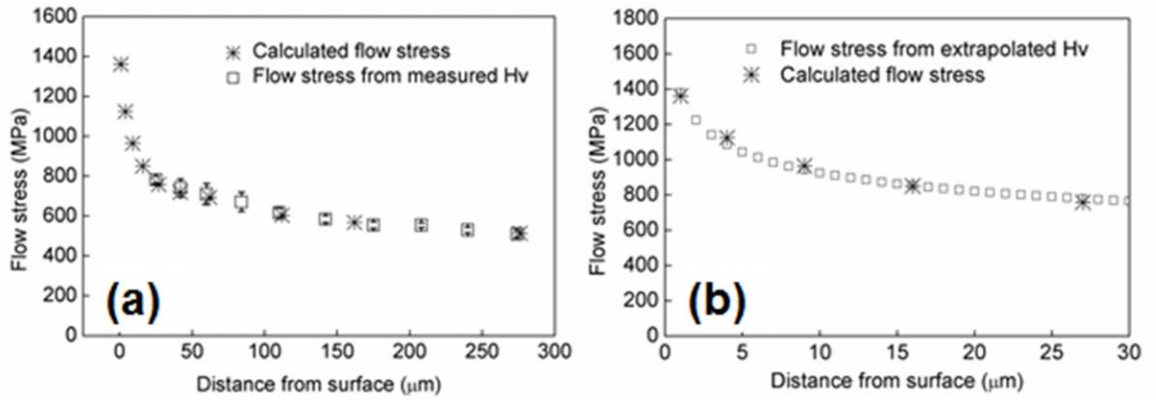

Figure 2. Calculated flow stress and measured flow stress based on microhardness (a) and its extrapolation (b) for the shot-peened low carbon steel. [4]

3.2 Compressed AA 1050 ring

In this experiment the objective is to investigate the stress distribution in a sample deformed heterogeneously. A six–step ring compression test was carried out, where the friction between the tool and the workpiece was maximized by choosing rough tools and poor lubrication, resulting in close to full sticking conditions (a friction factor of $f = 1$). Kerosene, commonly used for cleaning purposes, was used as a lubricant. The initial ring was prepared with an outer diameter of $D_0 = 18$ mm, an inner diameter of $d_0 = 9$ mm, and a height of $h_0 = 6$ mm.

Figure 3 shows the cross section of a ring compressed to a height reduction of 54.7 % (true strain of 0.6) where seven representative areas have been characterized by EBSD. The heterogeneous microstructure is pronounced, including (i) slightly deformed areas where the original grain shape is preserved and with a small amount of dislocation boundaries in the grains where the sticky zone is located (Area 3, figure 3d); (ii) compressed original grains with elongated dislocation boundaries in the grains (Area 7, figure 3h); (iii) equiaxed dislocation cells in the original grains [13, 14] (Area 2, figure 3c); (iv) equiaxed subgrains surrounded by low angle dislocation boundaries (Area 1, figure 3b); (v) inclined dislocation cell structures with one set of dense dislocation walls (DDWs) mixed with equiaxed dislocation cells (Area 5, figure 3f); (vi) inclined dislocation cell structures with two sets of DDWs dividing the original grains (Area 6, figure 3g); and (vii) parallel lamellar dislocation structures with shear bands (indicated by white arrows), which represent the microstructure typical of high strain deformation (Area 4, figure 3e). The average spacing between all boundaries, D_{av}, in each of these areas is shown in table 2. Note that Area 3, is almost undeformed, containing only the original grain boundaries, so the method based on deformation sub-grain structures is not applied here.

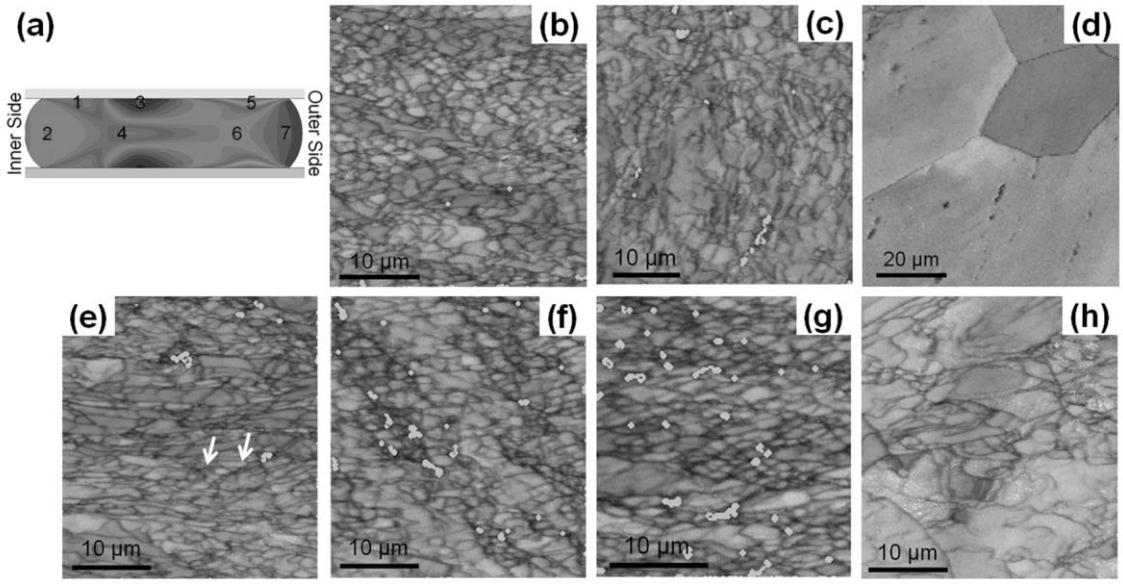

Figure 3. EBSD micrographs showing dislocation structures of the microstructure in the compressed AA 1050 ring. (b)-(h) show the microstructure of Areas 1-7 as marked in the simulated effective strain distribution map of the ring cross section (a).

Table 2. D_{av} of representative areas in the compressed AA 1050 ring

Position	Area 1	Area 2	Area 4	Area 5	Area 6	Area 7
D_{av} (µm)	0.95	1.05	0.74	0.84	0.85	1.21

In this study, the experimental analysis is validated by applying axisymmetric finite element modeling with the underlying calculations being built on the irreducible flow formulation, obtained by energy minimization. The material is assumed to be rigid-plastic and the tool is assumed to be perfectly rigid. For more details on the numerical implementation, see [15]. The friction model employed between the workpiece material and the tool surface is [16],

$$\tau = f\alpha k \tag{3}$$

where f is the friction factor to be calibrated, α is the ratio of real to apparent contact area, and k is the instantaneous shear flow stress obtained by the finite element simulation, taking strain hardening into account. The real contact area, is determined by an analytical expression suitable for finite element implementation [17].

For the seven areas, the calculated and simulated flow stresses are shown in table 3. The numbers are in good agreement taking into account an estimated standard deviation of around 6 %.

Table 3. Simulated strain, calculated flow stress (σ_{cal}) and simulated flow stress (σ_{simul}) of the seven representative areas in the ring (see figure 3).

Area	**2**	**1**	**4**	**3**	**6**	**5**	**7**
ε_{simul}	1.06	1.8	1.84	0.03	1.13	2.55	0.41
σ_{cal} **(MPa)**	127.1 ± 10.3	132.7± 10.8	147.9 ± 12.2	-	139.2 ± 11.4	140.1 ± 11.5	119.7 ± 9.6
σ_{simul} **(MPa)**	127.7	144.2	145	54.9	129.6	156.3	102.6

4. Discussion

This study encompasses four types of deformation microstructure, where two are homogeneous in rolled steel and compressed aluminum, and the other two are heterogeneous in shot-peened steel and friction deformed aluminum. All four structures are typical deformation microstructures subdivided by low and high angle dislocation boundaries. For all specimens except one, the effective strain is in the range from 1 to 5. The structure in each case is a bamboo structure [18] with extended medium and high angle boundaries (geometrically necessary boundaries (GNBs)) and interconnecting low angle boundaries (incidental dislocation boundaries (IDBs)). In previous analyses, the microstructure has been described in terms of the spacing between, and the misorientation across, the GNBs and IDBs as determined by TEM [3]. In the present more simple analysis, the structural parameters are quantified by EBSD where the angular resolution is ~ 1º and where the spacing between IDBs and GNBs, respectively is replaced by the average boundary spacing between all boundaries independent of the structural morphology.

In applying equation (2), it should be noted that k_2 is not constant, and may be expected in fact to increase with strain, due to an increase of θ^{LAB}, which is proportional to the square root of the strain [19]. However, at large strains an increased contribution from low-angle boundaries will be balanced by an increased fraction of high angle boundaries. As a result, k_2 is found not to be strongly dependent on the strain.

The local flow stress in the two heterogeneous structures has been validated by stress profiles obtained by microhardness measurements (for steel) and numerical simulation (for Al). A good agreement has been found supporting the application of equation (2) to a structural scale as low as about 50 nm. A further reduction in the structural scale down to or below ~10 nm requires an optimization of thermomechanical treatments and structural parameters. Example systems where such a scale may be reached include pearlitic steel wires [9, 11, 20-25], Cu alloyed with Fe [26] and Ni alloyed with Mo [27]. An extension of the present research will require a validation of the calculated stress profiles on an extremely fine scale together with mechanical testing at high spatial resolution, for example, in-situ TEM testing [28] and nano-indentation. However, such kinds of fine-scale testing also must take into account test specimen size effects or indentation size effects, to be analyzed in a forthcoming paper.

5. Conclusion

A microstructural method is described that allows the estimation of the local flow stress in a deformation microstructure, and its use has been demonstrated for two heterogeneous microstructures in steel and aluminium deformed to a maximum effective strain of 5 with a local structural scale as low as 50 nm. Based on this work the following conclusions can be made:

- The local flow stresses can be calculated with good accuracy based on microstructural parameters determined by EBSD, as demonstrated through a good agreement with microhardness measurements and with the results of numerical simulations.
- The microstructural method allows the flow stress distribution in a deformed sample to be determined in a precise manner, and can be used to underpin both analytical and numerical modelling, thereby finding applications in the design, processing and performance of metallic metals for engineering components.

Acknowledgements

The authors would like to thank The Danish Council for Independent Research (Grant number: DFF-1335-00230) for financial support.

References

[1] Hall E O 1951 *Proc. R. Soc. Lond. B.* **64** 747
[2] Petch N J 1953 J. Inst Steel Inst. **174** 25

[3] Hansen N 2004 *Scripta Mater.* **51** 801
[4] Zhang X, Hansen N, Gao Y and Huang X 2012 *Acta Mater.* **60** 5933
[5] Larson B C, Yang W, Ice G E, Budai J D and Tischle J Z 2002 *Nature* **415** 887
[6] Heilmann P, Clark W A T and Rigney D A 1983 *Acta Mater.* **31** 1293
[7] Taylor G L 1934 *Proc. R. Soc. Lond.*. **145** 362
[8] Kamikawa N, Huang X, Tsuji N, Hansen N 2009 *Acta Mater.* **57** 4198
[9] Zhang X, Godfrey A, Hansen N, Huang X, Liu W and Liu Q 2010 *Mater. Charac.* **61** 65
[10] Fan G H, Wang Q W, Du Y, Geng L, Hu W, Zhang X and Huang Y D 2014. *Materials Science and Engineering A* **590** 318.
[11] Zhang X, Godfrey A, Hansen N and Huang X 2013 *Acta Mater.* **61** 4898
[12] Zhu K N, Godfrey A, Hansen N and Zhang X D 2017 *Materials & Design* **117** 95
[13] Huang X and Hansen N 1997 *Scripta Mater.* **37** 1
[14] Le G M, Godfrey A, Hong C S, Huang X and Winther G 2012 *Scripta Mater.* **66** 359
[15] Nielsen CV, Zhang W, Alves L M, Bay N and Martins P A F 2013 *Modeling of thermoelectro-mechanical manufacturing processes with applications in metal forming and resistance welding*. Springer-Verlag, London, UK.
[16] Wanheim T and Bay N 1978 *Annals of the CIRP* **27** 189
[17] Bay N 1987 *Journal of Mechanical Working Technology* **14** 203
[18] Kuhlmann-Wilsdorf D and Hansen N 1991 *Scripta Metall. Mater.* **25** 1557.
[19] Pantleon W and Stoyan D 2000 *Acta Mater.* **48** 3005
[20] Zhang X D, Godfrey A, Liu W and Liu Q 2011 *Mater. Sci. Techno.* **27** 562
[21] Zhang X, Hansen N, Godfrey A and Huang X 2016 *Acta Mater.* **114**, 176
[22] Zhang X, Godfrey A, Huang X, Hansen N, Liu W and Liu Q 2014 *30th Risø International Symposium on Materials Science: Nanostructured metals: Fundamentals to applications (Risø, Denmark, 7-11 September 2014)* pp 409
[23] Zhang X, Hansen N, Godfrey A and Huang X 2014 *35th Risø International Symposium on Materials Science: New Frontiers of Nanometals (Risø, Denmark, 1-5 September 2014)* pp 153
[24] Zhang X, Godfrey A, Huang X, Hansen N and Liu Q 2011 *Acta Mater.* **59** 3422
[25] Li Y, Raabe D, Herbig M, Choi P-P, Goto S, Kostka A, Yarita H, Borchers C and Kirchheim R 2014 *Phys. Rev. Lett.* **113** 106104
[26] Hughes D A and Hansen N 2014 *Phys. Rev. Lett.* **112** 135504
[27] Hu J, Shi Y N, Sauvage X, Sha G and Lu K 2017 Science **355** 6331
[28] Zhang X, Godfrey A, Winther G, Hansen N and Huang X 2012 *Mater. Charac.* **70** 21